Density Functional Theoretical Investigations on Various Nanostructural Zeolite Surfaces

Gang Yang,* Xianchun Liu, Xiuwen Han, and Xinhe Bao*

State Key Laboratory of Catalysis, Dalian Institute of Chemical Physics, Chinese Academy of Sciences, 457 Zhongshan Road, Dalian 116023, P. R. China

Received: June 12, 2006; In Final Form: September 5, 2006

Through density functional calculations, the Brønsted acidities on various nanostructural ZSM-5 zeolite surfaces were studied as well as the hydrogen exchanging processes with adsorbed H_2O monomer or dimer. The Brønsted acidities on the four nanostructural surfaces show differences, although slightly, with their strengths increasing as (100) < (210) < (410) < (001). For hydrogen exchanging processes with H_2O monomer or dimer, the reaction rate increases in the order (210) < (100) < (001) < (410) or (210) < (410) < (001). No transition-state structure is present on H_2O dimer/(100) surface system. The introduction of a second H_2O molecule accelerates the hydrogen exchanging processes and meanwhile influences the nanostructural geometries such that they are more evident. Besides the activation barrier, the adsorption energy and reaction heat display differences from one surface to another, which results in the preference of catalytic reactions to a specific nanostructural zeolite surface, such as the hydrogen exchanging processes studied in this paper.

1. Introduction

As reviewed by Rolison,[1] heterogeneous catalysis is an inherently nanoscopic phenomenon with important technological and societal consequences for energy conversion and the production of chemicals. Actually, almost all the catalytic reactions proceed on nanostructural surfaces, and the surfaces along different directions will probably lead to notable selectivities to one specific catalytic process. There has been a great deal of experimental and theoretical efforts dedicated to understanding such phenomena.[2−6] Using scanning tunneling microscopy (STM), Wintterlin et al.[2] carefully studied the catalytic oxidation of CO by atomic O on nanostructural Pt-(111) surface. On the basis of the STM images within a specific (2×2) area along the reaction time, they obtained the reaction rates at several temperatures and the activation energy by Arrhenius plot. Duplock et al.[4] carried out first-principle calculations on perfect nanostructural graphene, concluding that the H_2 chemisorption is thermodynamically favorable on graphene by the combined effects of high curvature and Stone-Wales defect.

Nanostructural zeolite was and is considered by not a few researchers as the "philosopher's stone" of modern chemistry.[7] It has found great potential in heterogonous catalysis such as oil refining and fine chemicals manufacture, especially the ZSM-5 zeolite, a prototype of nanostructural zeolites. To zeolite catalysis, proton transferring from the Brønsted acidic site to the adsorbed molecule is a crucial step, which can be well investigated by probe molecules such as water, the most common and important adsorbent in zeolites.[8−10] With the aid of ab-initio molecular orbital calculations (Hartree−Fock and Møller−Plesset perturbation theories), Zygmunt et al.[10] studied the H−ZSM-5 zeolite clusters adsorbed with a single H_2O molecule, finding that two neutral complexes (hydrogen-bonded) locate at the local energy minima whereas the protonated complex acts as the transition state for the conversion between the two neutral complexes. As to the two H_2O molecules adsorbed on H−ZSM-5 zeolite, the definite viewpoint has not been reached yet as to whether the neutral or protonated complex dominates or coexists, which was elaborately described in previous research papers.[11−15]

To best of our knowledge, the differences in various nanostructural zeolite surfaces have never been reported, let alone their influences on the catalytic processes. Owing to the great importance and general interest, hydrogen exchanging processes between water and various ZSM-5 zeolite surfaces were chosen as the model reactions and were researched with first-principle density functional theory.

2. Calculation Details

Four nanostructural surfaces in ZSM-5 zeolite, that is, (001), (100), (210), and (410), along with the adsorbed molecules were investigated by means of density functional theory with BLYP functional, which includes the Becke exchange[16] and Lee, Yang, and Parr correlation functionals.[17] The (001), (100), (210), and (410) surfaces were represented by cluster models containing 14, 14, 16, and 13 T sites, respectively (see Figure 1). In each cluster, the atoms were made up of a closed zeolite pore, much larger than those of Rice et al. and Zygmunt and et al. with 5 T sites.[12,13] On the basis of previous experimental and theoretical results,[18,19] the Al atom in the zeolite surfaces occupies exclusively the T12 site. The boundary Si atoms were saturated by H atoms, which were oriented in the direction of what would normally be the next framework atoms. The corresponding Si−H distances were set to 1.500 Å. To retain the local structures of ZSM-5 zeolite and to save the computational resources, the atoms of $O_3Si-OH-AlO_3$ ($OH-AlO_3$ in the case of (410) surface) and adsorbed H_2O molecules were allowed to relax freely whereas the others were fixed at their Cartesian coordinates.

Density functional calculations at gradient-corrected approximation level were carried out under DMOL^3 program, CERIUS 2 of MSI.[20] The highly precise double numerical with polarization (DNP) basis set was adopted through the present

* Authors to whom correspondence should be addressed. E-mail: dblyyg@nefu.edu.cn (G.Y.); xhbao@dicp.ac.cn (X.B.).

10.1021/jp063664p CCC: $33.50
Published on Web 10/18/2006

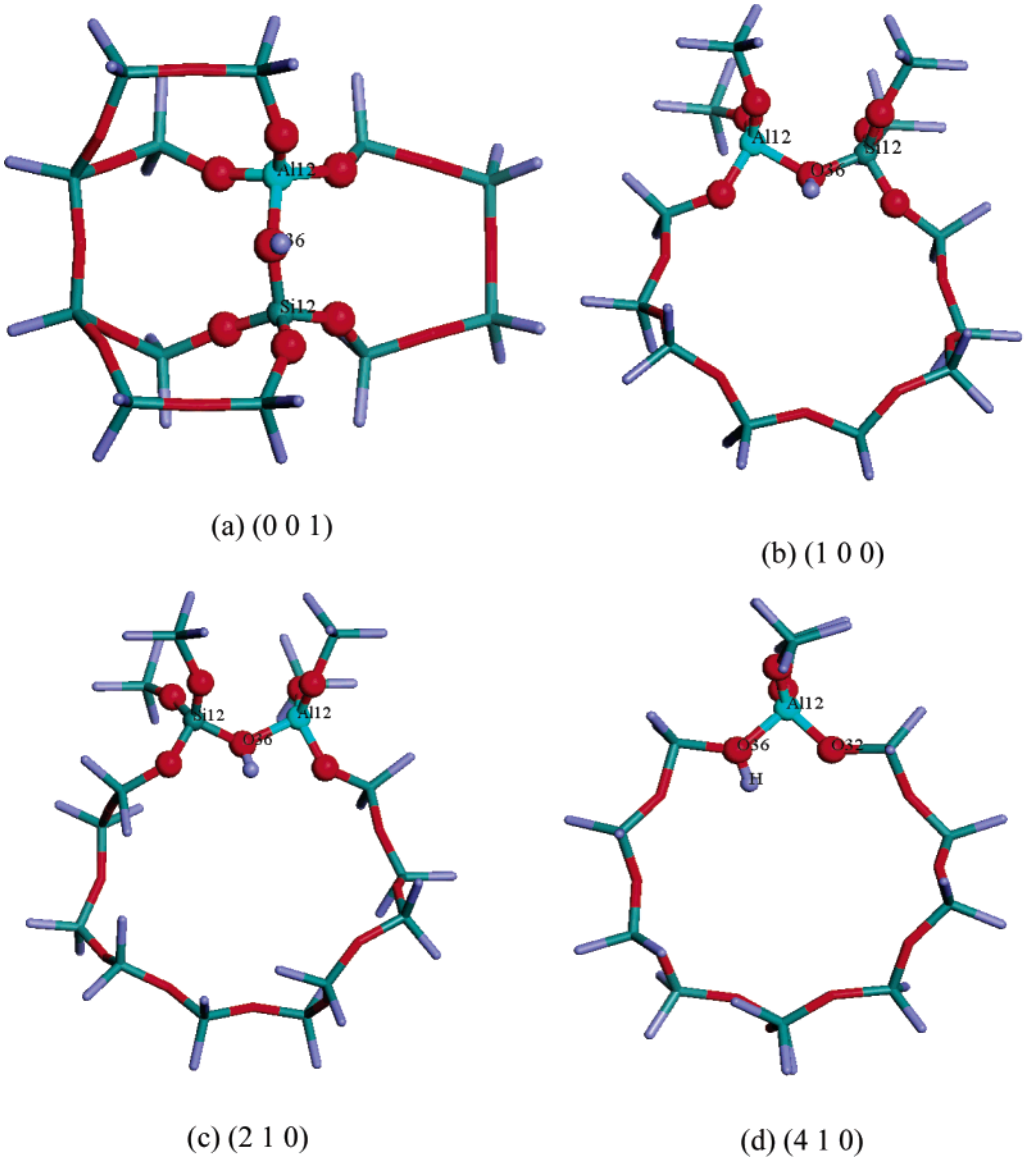

Figure 1. Local ZSM-5 zeolite structures along four different surfaces.

research, which proves even more reliable than the commonly used 6-31G(d, p) basis. To describe the structures of transition states and energy barriers as precisely as possible, the complete linear synchronous transit/quadratic synchronous transit (complete LST/QST) protocol in DMOL[3] module was employed for the transition-state searching.[21] Evaluations of molecular Hessians for the transition-state structures were performed confirming that the transition-state structures were characterized by only one imaginary frequency corresponding to the normal mode associated with the reaction coordinate.

As suggested by the referees, B3LYP functional under Gaussian03[22] was also employed to study the proton affinities of the four nanostructural surfaces. A 6-31G(d, p) basis was chosen to treat all the elements.

3. Results and Discussion

For convenience, the cluster models representing nanostructural surfaces of ZSM-5 zeolite were referred to $\Lambda(x\mathrm{H_2O}, lmn)$, where x denotes the number of probe molecule H_2O and l, m, and n are the Miller indexes of various ZSM-5 nanostructural surfaces. As there may exist several different stationary structures corresponding to each ($x\mathrm{H_2O}$, lmn), Λ was added ahead of ($x\mathrm{H_2O}$, lmn) for the differentiation, which equals **I**, **II**, and so forth.

3.1. Brønsted Acidic Proton. The $H-O_{36}$ distances were equilibrated at 0.976, 0.977, 0.977, and 0.980 Å in (001), (100), (210), and (410), respectively. The four values are close to each other and are consistent with previous theoretical data within the range of 0.970∼0.984 Å.[10,12,23,24] Differences in other geometric parameters were also observed in the four surfaces though slightly. For example, the $Si_{12}-O(H)-Al_{12}$ angles amount to 129.45°, 128.17°, 128.95°, and 129.14° in (001), (100), (210), and (410), respectively.

Generally, there are four parameters to characterize the strength of Brønsted acidity in zeolites: O−H bond length, charge on the acidic proton, proton affinity (PA), and O−H stretching frequency, of which proton affinity is acknowledged as the most accurate and powerful.[19,24,25] As depicted above, slight differences are present in the four O−H bond lengths. Theoretical errors considered, Mulliken charges on the acidic protons can be considered equivalent (see Table 1). Frequency calculations were performed on each optimized cluster of the zeolite surfaces. The values of O−H stretching frequencies were obtained and are listed in Table 1 without any scaling factor. It

TABLE 1: Brønsted Acidities along Different ZSM-5 Zeolite Surfaces[a]

	(001)	(100)	(210)	(410)
O−H/Å	0.976 (0.970)	0.977 (0.969)	0.977 (0.970)	0.980 (0.971)
Mulliken charge on H	0.345 (0.390)	0.345 (0.390)	0.345 (0.390)	0.351 (0.390)
ν(OH)/cm^{-1}	3642.1	3667.3	3663.2	3635.3
E_{dep}/kJ mol^{-1}	1216.7 (1256.4)	1236.5 (1278.2)	1232.5 (1274.4)	1230.0 (1270.6)
Si_{12}−O(H)−Al_{12}/deg	129.45 (130.87)	128.17 (129.42)	128.95 (130.16)	129.14 (130.23)

[a] The values in parentheses were obtained at B3LYP/6-31G(d, p) theoretical level under Gaussian03 program.

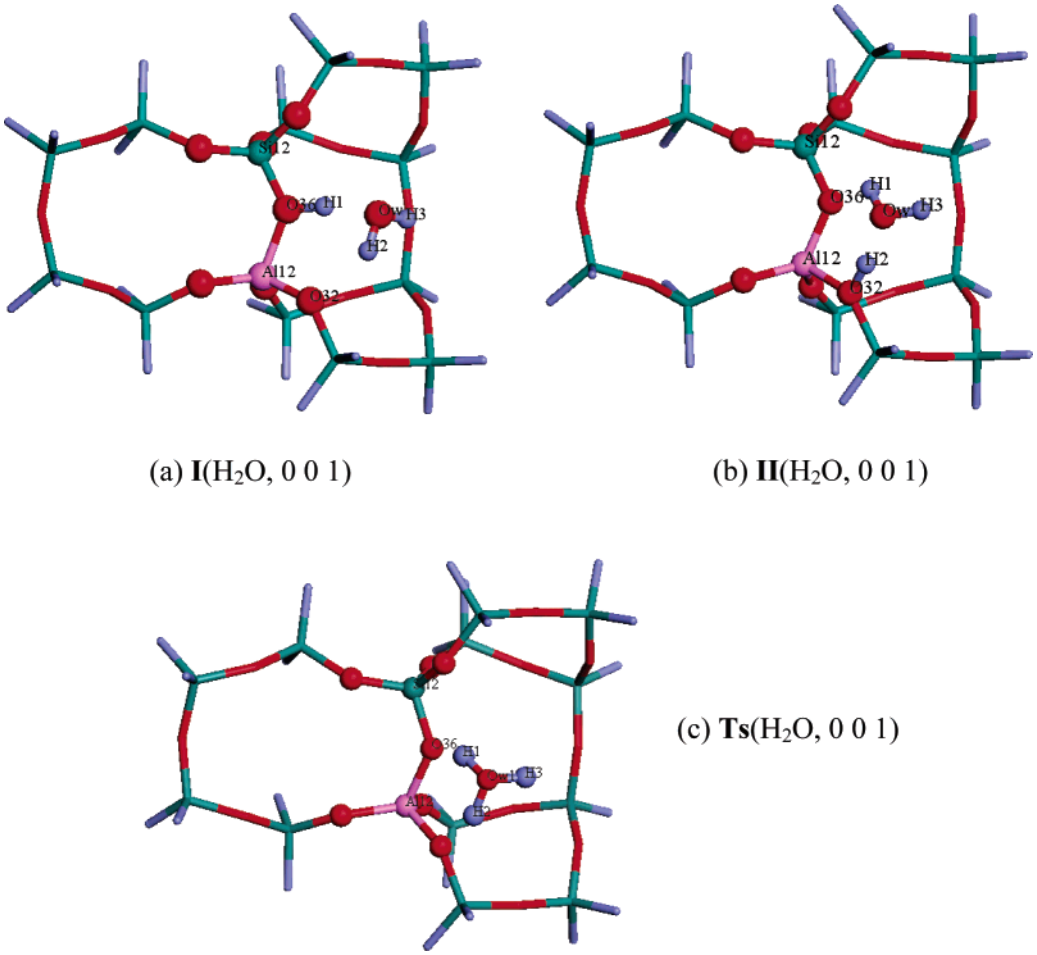

(a) **I**(H_2O, 0 0 1) (b) **II**(H_2O, 0 0 1)

(c) **Ts**(H_2O, 0 0 1)

Figure 2. Two local structures of (H_2O, 001) as well as their transition state.

was found that the O−H vibrational frequencies agree well with the experimental at 3612 cm^{-1} .[26] According to the O−H stretching frequencies, the Brønsted acidities of four nanostructural zeolite surfaces should increase in the order of (100) ≤ (210) < (001) ≤ (410).

The proton affinity of zeolite clusters can be estimated through the equation

$$\text{Zeo-O}-\text{H} \rightarrow \text{Zeo-O}^- + \text{H}^+ \quad (1)$$

$$E_{dep} = E(\text{Zeo-O}^-) - E(\text{Zeo-OH}) \quad (2)$$

where E(Zeo-OH) and E(Zeo-O$^-$) represent the energies of the zeolite clusters before and after deprotonation. With eq 2, the proton affinities were calculated to be 1216.7 kJ mol^{-1} for (001), 1236.5 kJ mol^{-1} for (100), 1232.5 kJ mol^{-1} for (210), and 1230.0 kJ mol^{-1} for (410), respectively. Zeolite surfaces with higher PA values are poorer proton donors and correspondingly have weaker Brønsted acidities. Accordingly, the strengths of the Brønsted acidity should change in the order (100) < (210) < (410) < (001). Divergences arise in the sequences of O−H stretching frequency and proton affinity. On the basis of previous results,[19,23,24] the proton affinity was set as the criterion to evaluate the Brønsted acidity. Therefore, the Brønsted acidities increase as (100) < (210) < (410) < (001).

B3LYP/6-31G(d, p) theoretical method under Gaussian03 program was also employed to study the proton affinities. As shown in the parentheses of Table 1, the proton affinities were calculated to be 1256.4 kJ mol^{-1} for (001), 1278.2 kJ mol^{-1} for (100), 1274.4 kJ mol^{-1} for (210), and 1270.6 kJ mol^{-1} for (410). Accordingly, the strength of Brønsted acidity should increase in the order (100) < (210) < (410) < (001), showing exactly the same sequence at BLYP/DNP theoretical level. In addition, the results at B3LYP/6-31G(d, p) theoretical level convince that the Brønsted acidity shows difference as the nanostructural zeolite surface is different.

3.2. H_2O Monomer as the Probe Molecule. For a single H_2O molecule adsorbed on the ZSM-5 zeolite surface, two neutral complexes were obtained as the local energy minima, shown in Figure 2. In **I**(H_2O, *lmn*), the acidic proton is directly bonded to the lattice O_{36} atom. The H_1−O_{36} distances in **I**(H_2O, 001), **I**(H_2O, 100), **I**(H_2O, 210), and **I**(H_2O, 410) were equili-

TABLE 2: Geometric Parameters Characterizing the Hydrogen Exchanging Processes of H_2O Monomer/ZSM-5 Surface System[a]

	H_1-O_{36}	H_1-O_w	H_2-O_w	H_2-O_{32}	H_3-O_w	$H_1-O_w-H_3$	$H_2-O_w-H_3$
I(H_2O, 001)	1.040	1.535	0.988	1.985	0.976	112.27	105.23
Ts(H_2O, 001)	1.483	1.080	1.034	1.538	0.996	114.28	112.45
II(H_2O, 001)	2.050	0.988	1.505	1.052	0.974	106.58	117.74
I(H_2O, 100)	1.045	1.534	0.986	2.016	0.975	115.63	106.69
Ts(H_2O, 100)	1.515	1.059	1.056	1.500	0.992	113.86	116.39
II(H_2O, 100)	1.914	0.991	1.486	1.063	0.975	106.31	115.64
I(H_2O, 210)	1.042	1.544	0.987	1.955	0.974	116.47	106.47
Ts(H_2O, 210)	1.528	1.041	1.063	1.510	1.000	114.84	114.43
II(H_2O, 210)	1.973	0.989	1.509	1.056	0.974	106.87	118.38
I(H_2O, 410)	1.055	1.504	0.988	1.983	0.974	116.87	107.00
Ts(H_2O, 410)	1.567	1.049	1.100	1.468	0.969	112.72	115.66
II(H_2O, 410)	1.993	0.989	1.521	1.051	0.974	106.50	117.01

[a] Bond length in Å and angle in degrees.

brated at 1.040, 1.045, 1.042, and 1.055 Å, respectively. Zygmunt et al.[10] carried out HF/6-31G(d) calculations on 8 T zeolite clusters, obtaining a smaller H−O distance at 0.98 Å. Our computational H−O distances are in fine agreement with the previous density functional value at ca. 1.05 Å on 5 T clusters reported by Rice et al.[12] and Krossner and Sauer[14] The values of H_2-O_w and H_3-O_w distances and $H_2-O_w-H_3$ angles indicate that the three atoms of H_2, O_w, and H_3 constitute one H_2O molecule (Table 2).

To one specific nanostructural zeolite surface, the adsorption energy of H_2O monomer can be obtained through the following equation:

$$E_{ad}(H_2O, lmn) = E(H_2O, lmn) - E(lmn) - E(H_2O) \quad (3)$$

where $E(H_2O, lmn)$ refers to the energy of the zeolite surface adsorbed with one H_2O molecule, and $E(lmn)$ and $E(H_2O)$ refer to the energies of the isolated zeolite surface and the H_2O molecule, respectively. The computational $E_{ad}(H_2O, lmn)$ values through eq 3 were equal to −53.6 kJ mol^{-1} on (001), −65.1 kJ mol^{-1} on (100), −59.4 kJ mol^{-1} on (210), and −61.6 kJ mol^{-1} on (410), agreeing well with the G2(MP2,SVP) value of −60.2 kJ mol^{-1} obtained with 8 T zeolite clusters.[10] Compared with previous theoretical results,[10,12−14] the $E_{ad}(H_2O, lmn)$ values of ours are the most close to the experimental values (−52.7 kJ mol^{-1} in ref 11 and −51.5 kJ mol^{-1} in ref 27), implying the role played by nanostructural zeolite surfaces when interacting with probe molecules such as water in this study.

The local structures of zeolite surfaces are highly stabilized by the complex hydrogen bonding. In **I**(H_2O, 001), the acidic proton forms a hydrogen bond with the O_w atom in the adsorbed H_2O molecule, and the mutual interaction leads to the slight elongation of H_1-O_{36} bond. The H_2 atom in the H_2O molecule forms hydrogen bond with the lattice O_{32}, and the H_2-O_{32} distance was optimized at 1.985 Å. It is somewhat larger than the theoretical value of 1.75 Å obtained by Rice et al.[12] The discrepancy was probably caused by the specific (001) surface. The H_2-O_{32} distances in the other three surfaces are close to the one in (001) surface. Analogous to the structures of **I**(H_2O, *lmn*), the geometric parameters of structures **II**(H_2O, *lmn*) vary somewhat from one nanostructural surface to another (see Table 2). In **II**(H_2O, *lmn*), the acidic proton is directly bonded to the O_{32} atom in zeolite lattice. The values of H_1-O_w and H_3-O_w bond lengths and $H_1-O_w-H_3$ angles reveal that the three atoms of H_1, O_w, and H_3 constitute one H_2O molecule.

The H_2O adsorption energies on the four **I**(*lmn*) or **II**(*lmn*) surfaces differ from one another, which causes the differences in the reaction heats to the nanostructural surfaces. The reaction heats of **I**(H_2O, *lmn*) converted into **II**(H_2O, *lmn*) can be computed with the aid of the equation

$$E_r(H_2O, lmn) = E[\mathbf{I}(H_2O, lmn)] - E[\mathbf{II}(H_2O, lmn)] \quad (4)$$

where $E[\mathbf{I}(H_2O, lmn)]$ and $E[\mathbf{II}(H_2O, lmn)]$ are the energies of the **I**(H_2O, *lmn*) and **II**(H_2O, *lmn*) zeolite clusters, respectively. The $E_r(H_2O, lmn)$ values were calculated to be −1.1, 11.6, 4.4, and 10.2 kJ mol^{-1} for (001), (100), (210), and (410), respectively.

On each specified zeolite surface, the ionic complex serves as the transition state for the two neutral complexes, see Figure 2c. The transition-state structure was referred to **Ts**(H_2O, *lmn*), with **Ts** added in front of the corresponding (H_2O, *lmn*) clusters. In **Ts**(H_2O, *lmn*), the O_w atom in the H_2O molecule forms direct bonds with three neighboring H atoms (H_1, H_2, and H_3), suggesting the formation of ionic H_3O^+ species (Table 2). Neither H_1 nor H_2 is directly bonded to the lattice O atoms; however, they form hydrogen bonding with the lattice O_{36} and O_{32} atoms, respectively. The H_1-O_{36} and H_2-O_{32} hydrogen bonds fall within the range of 1.47∼1.57 Å, larger than the MP2/6-31G(d) value of 1.36 Å obtained with fully optimized 3 T zeolite clusters.[10] The transition-state structures were stabilized by strong hydrogen bonding between the nanostructural zeolite surfaces and the adsorbed H_2O molecule. Frequency calculations were performed on these four transition-state structures, that is, **Ts**(H_2O, 001), **Ts**(H_2O, 100), **Ts**(H_2O, 210), and **Ts**(H_2O, 410). Each of them was characterized by only one imaginary frequency with the values at 352.2i, 287.7i, 412.3i, and 282.2i cm^{-1}, respectively. Through the transition-state structure containing the ionic H_3O^+ species, the neutral complex **I**(H_2O, *lmn*) can be converted into the other neutral complex **II**(H_2O, *lmn*).

The activation barrier [$E_{ac}(H_2O, lmn)$] is actually the energy difference between the transition-state structure **Ts**(H_2O, *lmn*) and the reactant **I**(H_2O, *lmn*). It amounts to 23.9, 28.0, 29.7, and 22.7 kJ mol^{-1} for (001), (100), (210), and (410), respectively. The activation barrier $E_{ac}(H_2O, lmn)$ increases as (410) < (001) < (100) < (210). In consequence, the hydrogen exchanging rates will differ in these four nanostructural ZSM-5 zeolite surfaces, and the zeolite surfaces show selectivities to the hydrogen exchanging processes. On the basis of the activation barriers, the reaction proceeds the fastest on (410) surface, then on (001) surface, then on (100) surface, and the slowest on (210) surface.

3.3. Introduction of a Second H_2O Molecule. In **I**($2H_2O$, 001), the acidic proton is directly bonded to O_{36} with the H_1-O_{36} distance of 1.114 Å, consistent with the value at 1.15 Å obtained at B3LYP/ 6-31G(d) theoretical level with 5 T zeolite

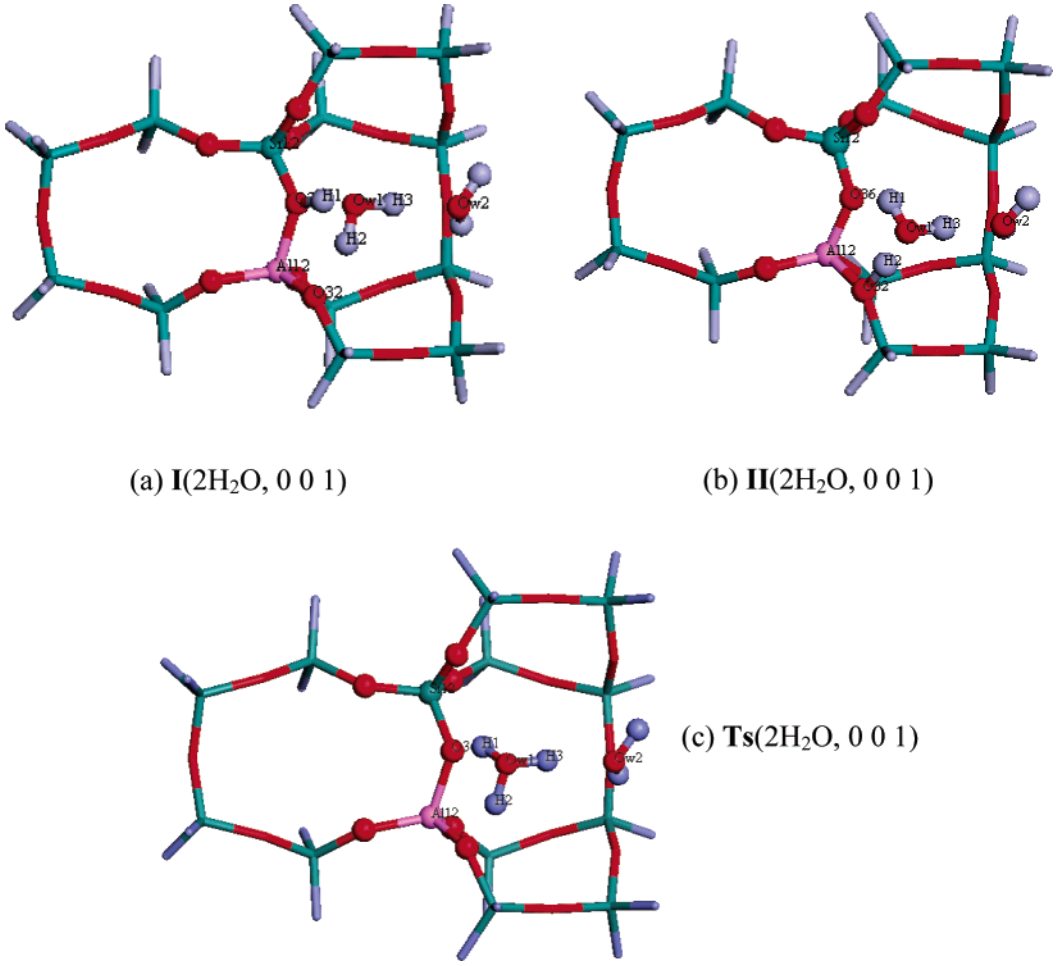

Figure 3. Two local structures of ($2H_2O$, 001) as well as their transition state.

TABLE 3: Geometric Parameters Characterizing the Hydrogen Exchanging Processes of H_2O Dimer /ZSM-5 Surface System[a]

	H_1-O_{36}	H_1-O_{w1}	H_2-O_{w1}	H_2-O_{32}	$H_1-O_{w1}-H_3$	$H_2-O_{w1}-H_3$	H_3-O_{w1}	H_3-O_{w2}
I($2H_2O$, 001)	1.114	1.365	0.985	2.045	108.66	104.99	0.999	1.770
Ts($2H_2O$, 001)	1.480	1.094	1.022	1.695	109.19	108.05	1.002	1.758
II($2H_2O$, 001)	2.014	0.989	1.296	1.163	104.54	107.41	1.001	1.751
I($2H_2O$, 210)	1.083	1.432	0.984	2.090	112.38	106.01	0.992	1.824
Ts($2H_2O$, 210)	1.483	1.078	1.017	1.672	112.55	110.30	1.007	1.824
II($2H_2O$, 210)	1.899	0.994	1.281	1.177	106.27	114.03	0.997	1.786
I($2H_2O$, 410)	1.132	1.343	0.990	1.906	114.81	106.84	0.994	1.811
Ts($2H_2O$, 410)	1.530	1.080	1.056	1.552	111.37	110.97	1.042	1.811
II($2H_2O$, 410)	1.883	0.996	1.263	1.188	107.21	114.32	0.997	1.775
I($2H_2O$, 100)	1.086	1.419	0.987	1.970	114.83	105.64	0.995	1.795

[a] Bond length in Å and angle in degrees.

clusters,[12] see Figure 3a. Owing to the attraction by the second H_2O molecule, the H_1-O_{36} value is larger than that in **I**(H_2O, 001). The acidic proton forms a hydrogen bond with the O_{w1} atom in the first H_2O molecule, and the H_2 atom in the first H_2O molecule is hydrogen bonded to the lattice O_{32} atom, see the exact values in Table 3. The local nanostructural ZSM-5 zeolite surfaces were highly stabilized by the complex hydrogen bonding between the adsorbed H_2O dimer and the zeolite surfaces as well as between the two H_2O molecules in the dimer. The values of H_2-O_{w1} and H_3-O_{w1} distances and $H_2-O_w-H_3$ angle show that the H_2, O_w, and H_3 atoms constitute a H_2O molecule. Meanwhile, the second H_2O molecule affords hydrogen bonding to the first H_2O molecule with the H_3-O_{w2} distance located at 1.770 Å. In **II**($2H_2O$, 001), the acidic proton is bonded to the lattice O_{32} atom with the distance of 1.163 Å. Hydrogen bonds form between the H_1 and O_{36} atoms and between the H_2 and O_{w1} atoms. The values of H_1-O_{w1} and H_3-O_{w1} distances and the angle of $H_1-O_{w1}-H_3$ suggest that the three atoms of H_1, O_{w1}, and H_3 constitute a H_2O molecule. Therefore, two neutral complexes with hydrogen bonding between the adsorbed H_2O molecules and (001) surface are present as the local energy minima. The same situations are applicable to the nanostructural (210) and (410) surfaces, where two hydrogen-bonded complexes were obtained as the local energy minima. On the (100) surface, however, only one stationary point **I**($2H_2O$, 100) was found through the continuous efforts of geometry optimizations. The acidic proton is connected with the lattice O_{36} atom with the distance at 1.086 Å. Potential energy surface was attempted to confirm that only one neutral complex is present on the (100) surface. By fixing the H_2-O_{32} distances at 1.000, 1.200, 1.400, 1.500, 1.600, 1.700, and 1.800 Å, geometry optimizations were performed on the H_2O dimer

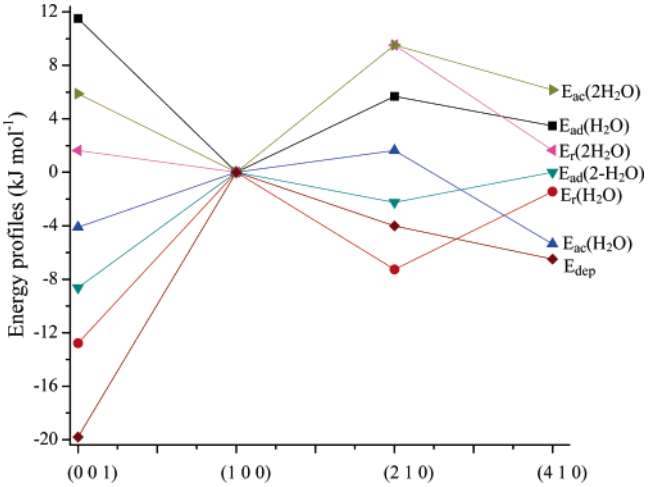

Figure 4. Relative energy profiles of adsorptions, activation barriers, and reaction heats for the hydrogen exchanging processes for H_2O monomer and dimer on four nanostructural zeolite surfaces (All the energies related with (100) surface were set to zero).

adsorbed on (100) surface. The corresponding H_1-O_{36} distances were optimized at 2.147, 1.884, 1.612, 1.501, 1.407, 1.315, and 1.109 Å, respectively. Compared to the stationary structure **I**($2H_2O$, 100), these structures are higher in energy by 15.1, 6.2, 3.5, 2.3, 1.8, 1.6, and 0.9 kJ mol^{-1}, respectively. It indicates that H_2O dimer/(100) surface system tends to be stabilized when the H_1 atom approaches the lattice O_{36} atom and that only one hydrogen-bonded complex is present for the H_2O dimer/(100) surface system. The adsorption energies of the second H_2O molecule [$E_{ad}(2\text{-}H_2O)$] are not as large as those of the first H_2O molecule,[12] with their values calculated at −46.0, −37.4, −39.6, and −37.4 kJ mol^{-1} on (001), (100), (210), and (410), respectively. The four $E_{ad}(2\text{-}H_2O)$ values were averaged to be −40.1 kJ mol^{-1} and are in fine agreement with the experimental value at −40.5 kJ mol^{-1}.[11] The previous theoretical results (Krosser and Sauer[14] at −59.7 kJ mol^{-1} and Rice et al.[12] at −49.3 kJ mol^{-1}) show relatively larger deviations from the experimental. The sequence of $E_{ad}(2\text{-}H_2O)$ follows as (410) ≈ (100) < (210) < (001), totally different from that of $E_{ad}(H_2O)$. It shows that the nanostructural zeolite surfaces exert some influence on the adsorption of both H_2O monomer and dimer. The reaction heats [$E_r(2H_2O)$] were calculated to be 1.6, 9.5, and 1.7 kJ mol^{-1} on (001), (210), and (410), respectively.

For the conversions from **I**($2H_2O$, *lmn*) to **II**($2H_2O$, *lmn*), the activation barriers [$E_{ac}(2H_2O)$] amount to 5.9, 9.5, and 6.2 kJ mol^{-1} on (001), (210), and (410), respectively. The $E_{ac}(2H_2O)$ values increase in the order (001) < (410) < (210). The $E_{ac}(2H_2O)$ values are much smaller than the corresponding $E_{ac}(H_2O)$, suggesting that the hydrogen exchanging processes are much speeded by the introduction of a second H_2O molecule. In the transition-state structures **Ts**($2H_2O$, *lmn*), the O_{w1} in the H_2O molecule forms three direct bonds with the H atom, see Figure 3c. Strong hydrogen bonding exists between the first and second H_2O molecule through the interaction of H_3 and O_{w2} atoms (Table 3). The H_2O dimer has a larger ability of capturing of hydrogen atoms than the single H_2O molecule and thus stabilizes the ionic transition-state structures.[13]

3.4. Sequences on the Four Nanostructural Zeolite Surfaces. Whether the nanostructural zeolite clusters have zero, single, or two H_2O molecules, the geometries of the four nanostructural surfaces show differences from one surface to another. As the result, the related energies will be different.

The Brønsted acidity in the four nanostructural surfaces increases as (100) < (210) < (410) < (001). Generally, the stronger the acidity, the higher the reactivity for this acidic proton. However, the present investigations of ZSM-5 zeolite surfaces adsorbed with H_2O molecules show that the viewpoint may not be correct because of the differences in the local geometries of the nanostructural zeolites.

Figure 4 clearly depicts the changing tendencies of the deprotonation energies, adsorption energies, reaction heats, and activation barriers for water adsorbed on the four nanostructural zeolite surfaces. The sequences of E_{dep}, $E_{ad}(H_2O)$, $E_r(H_2O)$, $E_{ac}(H_2O)$, $E_{ad}(2\text{-}H_2O)$, $E_r(2H_2O)$, and $E_{ac}(2H_2O)$ are (001) < (410) < (210) < (100), (001) < (210) < (410) < (100), (100) < (410) < (210) < (001), (410) < (001) < (100) < (210), (410) ≈ (100) < (210) < (001), (210) < (410) < (001) < (100), and (100) < (001) < (410) < (210), respectively. No two sequences are exactly the same. The adsorption energies, reaction heats, or activation barriers are neither in the same nor in the reverse sequences with that of deprotonation energies, that is, Brønsted acidities. The structural and energetic differences of adsorbents will determine which nanostructural surface is preferred for a specified catalytic process. One nanostructural zeolite, which is preferential for one catalytic reaction, may be inactive for another catalytic reaction.

4. Conclusions

In zeolites, the Brønsted acidity and reaction activity should be the invariant for the same T site. However, if the T site was located on different nanostructural zeolite surfaces, both the Brønsted acidity and reactivity will show differences from one surface to another, as was first explored in this paper through density functional theory calculations.

(1) The strengths of the Brønsted acidities on the four nanostructural surfaces show differences although slightly, which increase as (100) < (210) < (410) < (001).

(2) For the hydrogen exchanging processes between H_2O monomer and four different nanostructural surfaces, the reaction rate increases in the order (210) < (100) < (001) < (410).

(3) The introduction of a second H_2O molecule accelerates the hydrogen reaction rate. For H_2O dimer adsorbed on the four nanostructural surfaces, the reaction rate increases as (210) < (410) < (001). There is no transition-state structure present on H_2O dimer/(100) surface system.

(4) The influence of nanostructural zeolite surfaces on the hydrogen exchanging rates becomes more evident by the introduction of a second H_2O molecule, suggesting more dependence on the nanostructural surfaces.

(5) A specified catalytic reaction, including the hydrogen exchanging process presently investigated, may proceed preferentially on one nanostructural zeolite surface whereas be inhibited on another surface.

Acknowledgment. We gratefully acknowledged the financial support from the National Natural Science Foundation (No. 90206036).

References and Notes

(1) Rolison, D. R. *Science* **2003**, *299*, 1698−1701.

(2) Wintterlin, J.; Völkening, S.; Janssens, T. V. W.; Zambelli, T.; Ertl, G. *Science* **1997**, *278*, 1931−1934.

(3) Beck, R. D.; Maroni, P.; Papageorgopoulos, D. C.; Dang, T. T.; Schmid, M. P.; Rizzo, T. R. *Science* **2003**, *302*, 98−100.

(4) Duplock, E. J.; Scheffler, M.; Lindan, P. J. D. *Phys. Rev. Lett.* **2005**, *94*, 036104.

(5) Haase, F.; Sauer, J. *J. Am. Chem. Soc.* **1998**, *120*, 13503−13512.

(6) Michaelides, A.; Liu, Z. P.; Zhang, C. J.; Alavi, A.; King, D. A.; Hu, P. *J. Am. Chem. Soc.* **2003**, *125*, 3704−3705.

(7) Arends, I. W. C. E.; Sheldon, R. A.; Wallau, M.; Schuchardt, U. *Angew. Chem.* **2004**, *36*, 1144−1163 and references therein.

(8) Smith, L.; Cheetham, A. K.; Morris, R. R.; Marchese, L.; Thomas, J. M.; Wright, P. A.; Chen, J. *Science* **1996**, *271*, 799−802.

(9) Jobic, H.; Tuel, A.; Krossner, M.; Sauer, J. *J. Phys. Chem.* **1996**, *100*, 19545−19550.

(10) Zygmunt, S. A.; Curtiss, L. A.; Iton, L. X.; Erhardt, M. K. *J. Phys. Chem.* **1996**, *100*, 6663−6671.

(11) Olson, D. H.; Zygmunt, S. A.; Erhardt, M. K.; Curtiss, L. A.; Iton, L. E. *Zeolites* **1997**, *18*, 347−349.

(12) Rice, M. J.; Chakraborty, A. K.; Bell, A. T. *J. Phys. Chem. A* **1998**, *102*, 7498−7504.

(13) Zygmunt, S. A.; Curtiss, L. A.; Iton, L. X. *J. Phys. Chem. B* **2001**, *105*, 3034−3038.

(14) Krossner, M.; Sauer, J. *J. Phys. Chem.* **1996**, *100*, 6199−6211.

(15) Yang, G.; Wang, Y.; Zhou, D. H.; Liu, X. C.; Han, X. W.; Bao, X. H. *J. Mol. Catal. A: Chemical* **2005**, *237*, 36−44 and references therein.

(16) Lee, C.; Yang, W.; Parr, R. G. *Phys. Rev. B* **1988**, *37*, 785−789.

(17) Becke, A. D. *J. Chem. Phys.* **1988**, *88*, 2547−2551.

(18) Olson, D. H.; Khosrovani, N.; Peters, A. W.; Toby, B. H. *J. Phys. Chem. B* **2000**, *104*, 4844−4848.

(19) Redondo, A.; Hay, P. J. *J. Phys. Chem.* **1993**, *97*, 11754−11761.

(20) *CERIUS 2*, Version 4.2, DMOL 3; Molecular Simulations Inc., 2000.

(21) Gu, K. C.; Yang, G.; Zhang, W. P.; Yu, Z. K.; Han, X. W.; Bao. X. H. *J. Organomet. Chem.* **2006**, *691*, 1984−1992.

(22) Frisch, M. J.; Trucks, G. W.; Schlegel, H. B.; Scuseria, G. E.; Robb, M. A.; Cheeseman, J. R.; Montgomery, J. A., Jr.; Vreven, T.; Kudin, K. N.; Burant, J. C.; Millam, J. M.; Iyengar, S. S.; Tomasi, J.; Barone, V.; Mennucci, B.; Cossi, M.; Scalmani, G.; Rega, N.; Petersson, G. A.; Nakatsuji, H.; Hada, M.; Ehara, M.; Toyota, K.; Fukuda, R.; Hasegawa, J.; Ishida, M.; Nakajima, T.; Honda, Y.; Kitao, O.; Nakai, H.; Klene, M.; Li, X.; Knox, J. E.; Hratchian, H. P.; Cross, J. B.; Bakken, V.; Adamo, C.; Jaramillo, J.; Gomperts, R.; Stratmann, R. E.; Yazyev, O.; Austin, A. J.; Cammi, R.; Pomelli, C.; Ochterski, J. W.; Ayala, P. Y.; Morokuma, K.; Voth, G. A.; Salvador, P.; Dannenberg, J. J.; Zakrzewski, V. G.; Dapprich, S.; Daniels, A. D.; Strain, M. C.; Farkas, O.; Malick, D. K.; Rabuck, A. D.; Raghavachari, K.; Foresman, J. B.; Ortiz, J. V.; Cui, Q.; Baboul, A. G.; Clifford, S.; Cioslowski, J.; Stefanov, B. B.; Liu, G.; Liashenko, A.; Piskorz, P.; Komaromi, I.; Martin, R. L.; Fox, D. J.; Keith, T.; Al-Laham, M. A.; Peng, C. Y.; Nanayakkara, A.; Challacombe, M.; Gill, P. M. W.; Johnson, B.; Chen, W.; Wong, M. W.; Gonzalez, C.; Pople, J. A. *Gaussian 03*, revision C.02; Gaussian, Inc.: Wallingford, CT, 2004.

(23) Greatbanks, S. P.; Hillier, I. H.; Burton, N. A.; Sherwood, P. *J. Chem. Phys.* **1996**, *105*, 3770−3776.

(24) Chatterjee, A.; Chandra, A. K. *J. Mol. Catal. A* **1997**, *119*, 51−56.

(25) Sastre, G.; Fornes, V.; Corma, A. *J. Phys. Chem. B* **2002**, *106*, 701−708.

(26) Brand, H. V.; Redondo, A.; Hay, P. J. *J. Mol. Catal. A* **1997**, *121*, 45−62.

(27) Ison, A.; Gorte, R. J. *J. Catal.* **1984**, *89*, 150−158.